Predicting secondary electron emission rate in Hall Effect Thrusters

IEPC-2019-A-479

Presented at the 36th International Electric Propulsion Conference
University of Vienna, Austria
September 15-20, 2019

A. Tavant *
Safran Aircaft Engines, Vernon, France, and
LPP, CNRS, Ecole polytechnique, Sorbonne Universite, Univ. Paris-Sud, Observatoire de Paris, Universite Paris-Saclay, PSL Research University, 91128 Palaiseau
and

R. Lucken †, A. Bourdon ‡, and P. Chabert §

LPP, CNRS, Ecole polytechnique, Sorbonne Universite, Univ. Paris-Sud, Observatoire de Paris, Universite Paris-Saclay, PSL Research University, 91128 Palaiseau

The plasma-wall interaction in Hall Effect Thrusters (HETs) is discussed. New insights from Particle-in-Cell (PIC) simulations show that the electrons are not isothermal in the sheath when the neutral gas density is low. Using a polytropic state law for the electrons, we modify the sheath model with electron-induced secondary electron emission proposed by Hobbs (1967). We show that the improved sheath model allows us to predict accurately the secondary electron emission rate measured in the PIC simulations. It could explain the discrepancies between the experimental measurement and the simulations, and hence pave the way to more accurate HET modeling.

Nomenclature

σ	= secondary electron emission probability
σ_0	= minimum secondary electron emission probability
ϵ^*	= crossover energy
$\bar{\sigma}$	= secondary electron emission rate
$\epsilon = \frac{m_e}{2} v_e^2$	= electron energy, with m_e the electron mass and v_e the electron velocity
f	= electron distribution function
n_e	= electron density
p_e	= electron pressure
T_e	= electron temperature
e	=elementary charge
E_0	= axial electric field
B_0	= radial magnetic field
ϕ	= plasma potential
$\Delta\phi$	= plasma potential drop in the sheath
γ	= polytropic index

*Ph. D. student, antoine.tavant@lpp.polytechnique.fr
†Ph. D. student, romain.lucken@lpp.polytechnique.fr
‡Director of research at CNRS, anne.bourdon@lpp.polytechnique.fr
§Director of research at CNRS, pascal.chabert@lpp.polytechnique.fr

I. Introduction

WALL materials are known to affect the behavior and performances of the Hall Effect Thrusters (HET). [1,2] However, there is no proper understanding of the way the material changes the HET performances. Consequently, during the development of a HET either several wall materials are tested, hence increasing dramatically its cost and time, or only one material is used, therefore missing a possible more effective thruster configuration. A better understanding of the plasma-wall interaction is needed to improve the HET understanding and performances.

The main physical phenomena proposed to explain the observed impacts of the wall material on the HET is the secondary electron emission (SEE) induced by electron impact. Recent particle in cell (PIC) simulations [3] have shown that the SEE does not necessarily affect the electron cross-field transport which comes from predominantly both the azimuthal instability and the electrons-wall collisions. On the other hand, an increase of the SEE yield can reduce the sheath potential drop at the wall, hence increasing the electron power losses. While this observation has already been made in both experiments [4] and fluid simulations, [5] a significant discrepancy lies between the two. In this work, we present new insights from a 2D PIC simulation, and propose a new sheath model to better predict the SEE rates.

II. Bi-dimensional radial-azimuthal PIC simulations

In this work, simulations are carried out with the Particle-In-Cell (PIC) simulation code, LPPic, developed at LPP. This code has been used in several studies on low temperature low pressure plasmas. [8–13] More details on its implementations, performances, and validation can be found elsewhere. [7]

A. Presentation of the 2D PIC simulations

The radial-azimuthal exit plane of a HET is modeled using a 2D PIC simulation. The channel curvature is neglected, hence a Cartesian mesh is used. A uniform axial electric field E_0 and a uniform radial magnetic field B_0 are fixed. Figure 1 gives a schematic representation of the simulation domain. The radial length is $L_R = 2$ cm, and the azimuthal length is $L_\theta = 0.5$ cm. Is overlaid the radial-azimuthal distribution of the electron density n_e. We see in Fig. 1 the azimuthal instability on n_e, which wavelength is of the order of the millimeter. The axial convection is modeled by fixing a finite length L_Z in the third direction. Particles exiting the axial domain are removed, and new particles are generated to conserve the quasineutrality. We use $L_Z = 1$ cm. Ionization is not self-consistently modeled, but instead, we use a fixed ionization rate to balance the radial losses. Consequently, the plasma density remains constant, and the simulations converge after a few microseconds toward a steady state.

The radial boundaries are grounded, but they do not drive current. Thus, a floating sheath self-consistently forms to obtain the charge conservation in the plasma. The secondary electron emission is modeled using a linear law for the emission probability. [5] When an electron reaches the wall, the probability of emission is

$$\sigma(\epsilon) = \begin{cases} \sigma_0 + (1-\sigma_0)\frac{\epsilon}{\epsilon^*} & \text{if } \epsilon < \epsilon_{\max} \\ \sigma_{\max} & \text{if } \epsilon \geq \epsilon_{\max} \end{cases} \tag{1}$$

where $\epsilon = \frac{m_e}{2} v_e^2$ is the kinetic energy of the primary incoming electron, σ_0 is the asymptotic probability of emission at energy null, ϵ^* is the crossover energy above which the probability of emission is higher that one, $\sigma_{\max}$is the maximum probability and $\epsilon_{\max} = \frac{\sigma_{\max}-\sigma_0}{1-\sigma_0}\epsilon^*$ is the minimum energy for which $\bar{\sigma} = \sigma_{\max}$. The emission rate $\bar{\sigma}$ corresponds to the emission probability averaged over the electron flux

$$\bar{\sigma} = \frac{\iiint_{\mathbf{v_e}\cdot\mathbf{n}>0} v_x \sigma(\mathbf{v_e}) f(\mathbf{v_e}) d^3v}{\iiint_{\mathbf{v_e}\cdot\mathbf{n}>0} v_x f(\mathbf{v_e}) d^3v}$$

with $\mathbf{v_e}$ the electron velocity vector, f the electron velocity distribution function, and $\mathbf{n}$ the unit vector normal to and toward the wall. With a Maxwellian distribution function of temperature T_e, neglecting the saturation at $\sigma_{\max}$, we obtain

$$\bar{\sigma}_{\mathrm{Maxw}} = \sigma_0 + (1-\sigma_0)\frac{2\mathrm{T}_e}{\epsilon^*}. \tag{2}$$

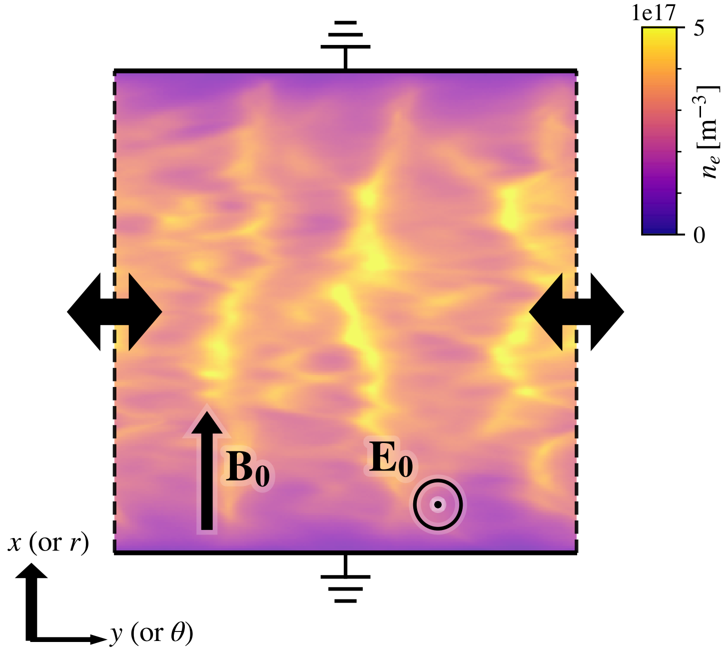

Figure 1. Schematic representation of the radial-azimuthal simulation domain. Overlaid is the electron density n_e given as an example. The radial length is 2 cm, and the azimuthal length is 0.5 cm. The magnetic field is $B_0 = 0.02$ T, the axial electric field is $E_0 = 2{\times}10^4$T, and the walls are grounded.

We recall that if the emission rate $\bar{\sigma}$ is too large, the sheath enter the Space Charge Limited regime (SCL). [6] In this regime, a potential well forms close to the wall so that emitted electron are reflected to the wall. Therefore, the effective rate is limited to the critical value $\bar{\sigma}_{\rm cr} \simeq 0.983$ for a xenon plasma.

B. Simulation result

We use the SEE parameters $\epsilon^* = 50$ V and $\sigma_0 = 0.5$, which are on the order of those for the typical ceramic used in HETs. Table 1 presents the results of the simulation for the electron temperature and the SEE rate measured $\bar{\sigma}_{PIC}$. The value of Eq. (2), using the electron temperature measured T_e is also given.

Table 1. Results of the 2D PIC simulation, averaged over the whole simulation domain and in time over 5μs during the steady state.

Parameter	Value
Electron temperature T_e	48.3 V
SEE rate $\bar{\sigma}_{PIC}$	0.85
Results of Eq. (2) $\bar{\sigma}_{th}$	1.37

We can see that the prediction of Eq. (2) overestimates the SEE rate, compared to the values measured in the 2D PIC simulations. This discrepancy is similar to the one noted by Raistes et al. (2005) [6] between fluid models and experimental measurements. In order to explain the discrepancy between the SEE rate measured and the theory, Figure 2 shows the radial profile of the electron temperature averaged in time over 5μs and in the azimuthal direction.

We see in Fig. 2 that the electron temperature is not uniform, but instead decreases drastically from the plasma bulk to the wall. Therefore, the isothermal hypothesis do not stand. In addition, it could explain the reason why the SEE rate observe in the simulation is lower than the PIC simulations.

Figure 3 shows, the evolution in logarithmic scale of the electron pressure $p_e = n_e e \mathrm{T}_e$, with n_e the

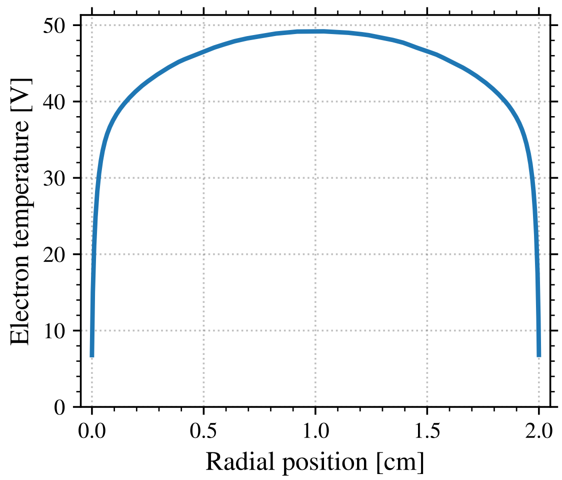

Figure 2. Radial profile of the electron temperature averaged in the azimuthal direction, and in time over 5μs during the steady state.

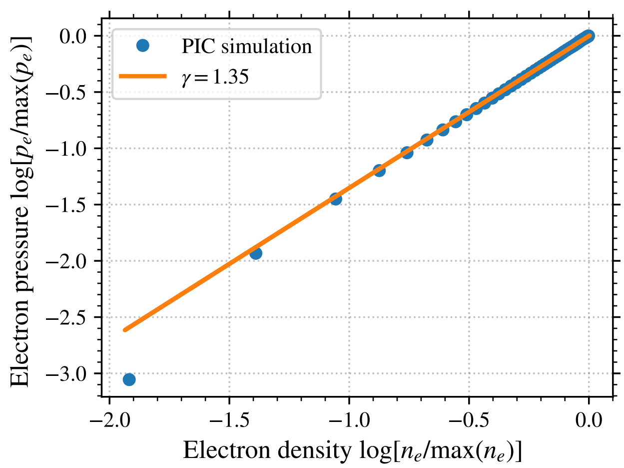

Figure 3. Evolution in logarithmic scale of the electron pressure $p_e = n_e e \mathrm{T}_e$, with n_e the electron density and e the elementary charge, as a function of n_e at each radial position. The markers correspond to the PIC simulation results (one marker every ten cells), and the line corresponds to a linear fit, which constant of proportionality γ is given in the legend.

electron density and e the elementary charge, as a function of n_e at each radial position. We can see that the evolution in log scale of p_e is proportional to n_e, which corresponds to the polytropic state law:

$$\nabla \left(p_e n_e^{\gamma}\right) = 0, \tag{3}$$

with γ the polytropic index. The value of γ measured in the PIC simulations is $\gamma = 1.35$. Using the electron momentum conservation equation

$$\nabla(n_e \mathrm{T}_e) - n_e \nabla\phi = 0, \tag{4}$$

with ϕ the plasma potential, the polytropic state law results in

$$\nabla \mathrm{T}_e = \frac{\gamma - 1}{\gamma} \nabla\phi \tag{5}$$

which explains the radial profile of the electron temperature. In the next section, we use Eq. (5) to close the electron set of equations in the sheath model.

III. Sheath model with Secondary Electron Emission and polytropic electrons

We suppose the sheath collisionless. The floating sheath forms so that we obtain the current equality at the wall

$$\Gamma_i = (1-\bar{\sigma})\Gamma_e, \tag{6}$$

with Γ_i and Γ_e the ion and electron fluxes, respectively. The ion flux is conserved in the sheath (there is no ionization), hence we have the modified Bohm flux for polytropic electrons [11]

$$\Gamma_i = n_0\sqrt{\frac{\gamma e \mathrm{T}_{e0}}{m_i}}, \tag{7}$$

with the subscript 0 designing the sheath edge. The electron flux at the wall is a thermal flux, with the electron density and temperature at the wall

$$\Gamma_e = \frac{1}{4} n_{e,w}\sqrt{\frac{8e\mathrm{T}_{e,w}}{\pi m_e}}. \tag{8}$$

The electron density $n_{e,w}$ and temperature $\mathrm{T}_{e,w}$ at the wall are related to the sheath edge values with Eqs. (4) and (5). We obtain the equation for the plasma potential drop from the sheath edge to the wall $\Delta\phi$

$$(1-\bar{\sigma})\left[1+\frac{\gamma-1}{\gamma}\frac{\Delta\phi}{\mathrm{T}_{e0}}\right]^{\frac{1}{\gamma-1}}\sqrt{1-\frac{\gamma-1}{\gamma}\frac{\Delta\phi}{\mathrm{T}_{e0}}} = \sqrt{\frac{4\gamma\pi m_e}{m_i}} \tag{9}$$

We solve Eq. (9) to obtain the potential drop $\Delta\phi$ as a function of the electron temperature at the sheath edge T_{e0}. The SEE rate $\bar{\sigma}$ is obtained with Eq. (2) with the electron temperature at the wall $\mathrm{T}_{e,w}$, and with a saturation at $\bar{\sigma}_{cr}$. Figure 4 shows the solution $\Delta\phi$ as a function of the electron temperature.

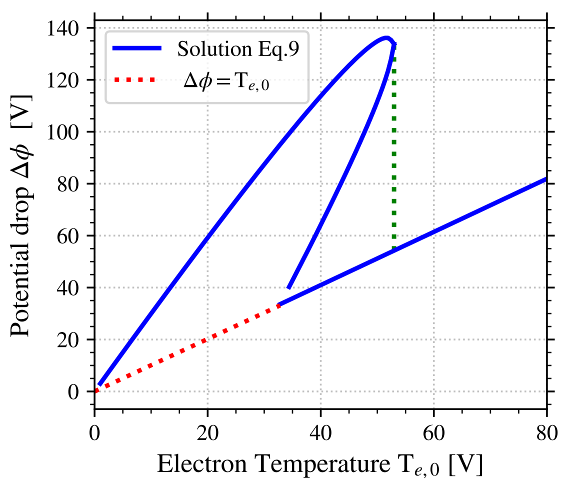

Figure 4. Potential drop between the sheath edge and the wall as a function of the electron temperature at the sheath edge T_{e0}, obtained by solving Eq. 9.

We see that Eq. (9) resents up to three solutions between $\mathrm{T}_e = 35$ and 55 V. This is because both the SEE rate $\bar{\sigma}$ and the primary electron flux Γ_e depend on the plasma potential. For $\mathrm{T}_e = 48.3$ V (value measured in the PIC simulation), we read $\Delta\phi = 49.4, 102.7$ and 132.2 V.

The three solutions obtained correspond to three different states of the sheath. We can expect that starting the simulation from a low value of T_e and heating the electrons, the sheath would remain in the same state until the threshold temperature value $\hat{\mathrm{T}}_e = 55$ V is reached. Then, the sheath would jump the other state. Therefore, for $\mathrm{T}_e = 48.3$ V the sheath remains on the upper branch. In this case, using Eq. (5) we obtain $\mathrm{T}_{e,w} = 14$ V, hence $\bar{\sigma}_{th} = 0.8$, in better agreement with $\bar{\sigma}_{PIC}$ than using the isothermal hypothesis.

IV. Conclusion

Using 2D PIC radial-azimuthal PIC simulations, we observe a large discrepancy between the electron-induced secondary electron emission rate measured in the simulation and the theoretical value. We show that the origin of the discrepancy is the evolution of the electron temperature in the sheath, which is not isotherm. On the contrary, the electrons follow a polytropic state law, which polytropic index is close to $\gamma = 1.35$.

Using the polytropic state law, we derive a new sheath model that takes into account the secondary electron emission. This modified sheath model allows us to accurately obtain the emission rate measured in the PIC simulation. This new sheath model may explain the discrepancies observed between the experimental measurement and the models. The modified sheath model requires one new parameter: the polytropic index γ for the electrons, that depends exclusively on the electron velocity distribution function. [11] This parameter could be determined by radially resolved measurements of T_e and n_e, measurement of the electron velocity distribution function, or via kinetic models (Monte Carlo model, Direct kinetic simulations, or with analytic approaches).

Lastly, the model presented here has to be coupled with the neglected effects of magnetic mirrors and the channel curvature. [14]

Acknowledgments

The authors thank J.L Raimbault for helpful discussions on this work. A. Tavant acknowledges financial and technical support from a Safran Aircraft Engines doctoral research award. This work has been partially funded by ANR (no. ANR-16-CHIN-003-01) and Safran Aicraft Engines with the project POSEIDON. This work was granted access to the HPC resources of CINES under the allocation 2018-A0040510092 made by GENCI, and the resources of CERFACS.

References

[1] D. M. Goebel, I. Katz, *Fondamentals of Electric Propulsion : Ion and Hall Thrusters*, JPL Space Science and Technology Series (2008).

[2] N. Gascon and M. Dudeck and S. Barral, 'Wall material effects in stationary plasma thrusters. I. Parametric studies of an SPT-100', Phys. Plasmas, vol. 10, no. 10, p. 4123-4136, 2003

[3] A. Tavant, V. Croes, R. Lucken, T. Lafleur, A. Bourdon, and P. Chabert, 'The effects of secondary electron emission on plasma sheath characteristics and electron transport in an $\mathbf{E} \times \mathbf{B}$ discharge via kinetic simulations', Plasma Sources Sci. Technol., vol. 27, no. 12, p. 124001, 2018.

[4] Y. Raitses, A. Smirnov, D. Staack, and N. J. Fisch, 'Measurements of secondary electron emission effects in the Hall thruster discharge', Phys. Plasmas, vol. 13, no. 1, p. 014502, Jan. 2006.

[5] S. Barral and K. Makowski and Z. Peradzyński and N. Gascon and M. Dudeck, 'Wall material effects in stationary plasma thrusters. II. Near-wall and in-wall conductivity' , Phys. Plasmas, vol. 10, no. 10, p. 4137-4152, 2003.

[6] Y. Raitses, D. Staack, M. Keidar, and N. J. Fisch, 'Space charge saturated sheath regime and electron temperature saturation in Hall thrusters', Phys. Plasmas, vol. 12, no. 7, p. 073507, 2005

[7] A. Tavant, 'Plasma-wall interaction and electron transport in Hall Effect Thrusters', Ph.D. thesis, 2019

[8] V. Croes, T. Lafleur, Z. Bonaventura, A. Bourdon, and P. Chabert, '2D Particle-in-Cell Simulations of the Electron Drift Instability and Associated Anomalous Electron Transport in Hall-Effect Thrusters', Plasma Sources Sci. Technol., vol. 26, no. 3, p. 034001, 2017.

[9] V. Croes, A. Tavant, R. Lucken, R. Martorelli, T. Lafleur, A. Bourdon, and P. Chabert, 'The Effect of Alternative Propellants on the Electron Drift Instability in Hall-Effect Thrusters: Insight from 2D Particle-in-Cell Simulations', Physics of Plasmas, vol. 25, no. 6, p. 063522, 2018.

[10] A. Tavant, R. Lucken and A. Bourdon, and P. Chabert, 'The Effects of Secondary Electron Emission on Plasma Sheath Characteristics and Electron Transport in an E x B Discharge via Kinetic Simulations ', Plasma Sources Sci. Technol., vol. 27, no. 12, p. 124001, 2019.

[11] A. Tavant, R. Lucken and A. Bourdon, and P. Chabert, 'Non-Isothermal Sheath Model for Low Pressure Plasmas ' Plasma Sources Sci. Technol., vol. 28, no. 7, p. 075007, 2019.

[12] R. Lucken, V. Croes, T. Lafleur, J.-L. Raimbault, A. Bourdon, and P. Chabert, 'Edge-to-Center Plasma Density Ratios in Two-Dimensional Plasma Discharges' Plasma Sources Sci. Technol., vol. 27, no. 3, p. 035004, 2018.

[13] R. Lucken, V. Croes, T. Lafleur, J.-L. Raimbault, A. Bourdon, and P. Chabert, 'Instability-Enhanced Transport in Low Temperature Magnetized Plasma' Physics of Plasmas, vol. 26, no. 7, p. 070702, 2019.

[14] A. Domínguez-Vázquez, F. Taccogna, and E. Ahedo, 'Particle modeling of radial electron dynamics in a controlled discharge of a Hall thruster', Plasma Sources Sci. Technol. 27, 064006, 2018.